Power Flow and Inductor Current Analysis of PWM Control for Dual Active Bridge Converter

Anping Tong[1,2], Lijun Hang[1,2], Guojie Li[1,2], Yajuan Guo[3], Yunfeng Zou[3], Jinming Chen[3], Jun Li[4], Jian Zhuang[5], Siwei Li[6]

1. Key Laboratory of Control of Power Transmission and Conversion (Shanghai Jiao Tong University), Ministry of Education
2. Dept. of Electrical and Electronic Engineering, Shanghai Jiao Tong University, Shanghai 200240, China
3. State Grid Jiangsu Electric Power Company Electric Research Institute
4. Zhejiang Jiaxing Electricity Bureau, Jiaxing 314000, China
5. State Grid Tianjin Electric Power Corporation, Beijing 300384, China;
6. Beijing Guodiantong Network Technology Co., Ltd, Beijing 100070, China

tonganping@sjtu.edu.cn

***Abstract*—PWM control method is an important method for the optimization operation of Dual Active Bridge (DAB) converter. The traditional way which is used to analyze PWM control is not precise and comprehensive. This paper gives the accurate calculation of power flow and RMS value of inductor current by proposing a novel method. Six modes are analyzed based on the control signal distributions. Finally, the simulations and experiments are used to verify the theoretic results.**

Keywords—DAB; single-phase-shift (SPS); dual-phase-shift (DPS); triple-phase shift (TPS).

I. INTRODUCTION

DAB-IBDC (Dual Active Bridge-Isolated Bidirectional DC/DC converter) was first proposed by Kheraluwala [1]. The basic topology of DAB-IBDC which combines two single phase H bridges with a single phase high frequency transformer is showed in Fig. 1. An inductor is needed for current limitation, and the inductor also influences the power transmission of DAB-IBDC. Due to the advantages of high power density, soft switching properties, and bidirectional power flow capability, DAB-IBDC has been expected to be employed in battery energy storage systems and renewable energy sources, which will be integrated into the smart grid [2].

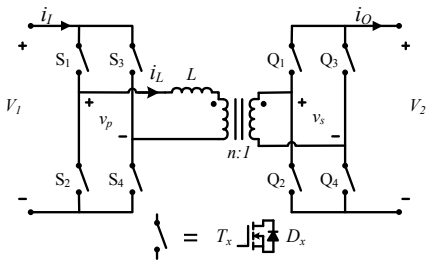

Fig.1 Basic topology of DAB-IBDC

In Fig. 1, the output of the primary side H bridge is v_p(t) , and the output of the secondary side H bridge is v_s(t). The i_L(t) represents the current flowing through the inductor *L*. *L* can be the leakage inductor of the high frequency transformer with turn ratio *n*, or be an individual inductor.

Control method is an important research direction for DAB-IBDC [3]. Phase shift control is the most commonly used control method for DAB-IBDC. According to the number of control degrees, phase shift control can be simply classified as single-phase-shift (SPS), dual-phase-shift (DPS), and triple-phase shift (TPS). It is the simplicity of SPS control that makes this control method been widely used. Disadvantages of the SPS control are the limited operation range and a large amount of reactive power that may occur at certain working point [4]. The DPS control method is proposed to reduce the current stress, and eliminate the reactive power [5]. However, this scheme can only get the relative optimized solution at some working points, and the efficiency can be improved further. The TPS control method which is also called PWM control method is the unified form of phase-shift-control [3]. The SPS control and DPS control can be regarded as special cases of TPS control [3]. Theoretically, the global optimized solution for every working point can be got by this control scheme.

Because of the complexity of calculation, some simplified methods are developed to analyze the PWM control for DAB-IBDC, such as fundamental component analysis [6], [7]. But these ways for PWM control analysis are not accurate. This paper proposes a novel method that is based on the superposition principle of the circuits to analyze and calculate the PWM control of DAB-IBDC accurately. Six modes are analyzed based on the control signal distributions. The proposed method takes advantages in reducing complexity of calculation significantly, and more physical insight can be obtained. Finally, the simulations and experiments are used to verify the theoretic results.

II. PWM CONTROL METHOD

A. The Basic Operation of PWM Control Method

A typical waveform of PWM control for DAB converter is shown in Fig. 2. As in Fig. 2., the gate signals of switching

This paper and its related research are supported by grants from the Power Electronics Science and Education Development Program of Delta Environmental and Education Foundation under Grant DREG2015005, and National High Technology Research and Development Program of China 863 Program (2014AA052003), and the Natural Science Foundation of Shanghai Science and Technology Commission under Grant 14ZR1422200.

978-1-5090-1210-7/16/$31.00 ©2016 IEEE

978-1-5090-1210-7/16/$31.00 ©2016 IEEE

devices S_1-S_4 and Q_1-Q_4 are square waves with 50% duty ratio for the corresponding switches. There are three types of phase shift among S_1-S_4 and Q_1-Q_4 gate signals. For the so-called PWM control method, the phase shift, which is between $v_p(t)$ and $v_s(t)$, and the corresponding phase shifts in both the primary side H bridge and secondary side H bridge can be adjusted independently. Then three degrees of freedom can be controlled. This is the reason why PWM control method can be called TPS control method.

In Fig. 2, T is the half switching period, then $f_s = 1/(2T)$, f_s is the switching frequency of DAB-IBDC. D_1T is defined as the phase shift in the primary H bridge, so 1-D_1 is the duty ratio of $v_p(t)$; and D_2T is the phase shift in the secondary H bridge, therefor 1-D_2 is the duty ratio of $v_s(t)$; and D_0T is the phase shift between $v_p(t)$ and $v_s(t)$. For PWM control method, D_0, $D_1$and D_2 can be the arbitrary values from 0 to 1.

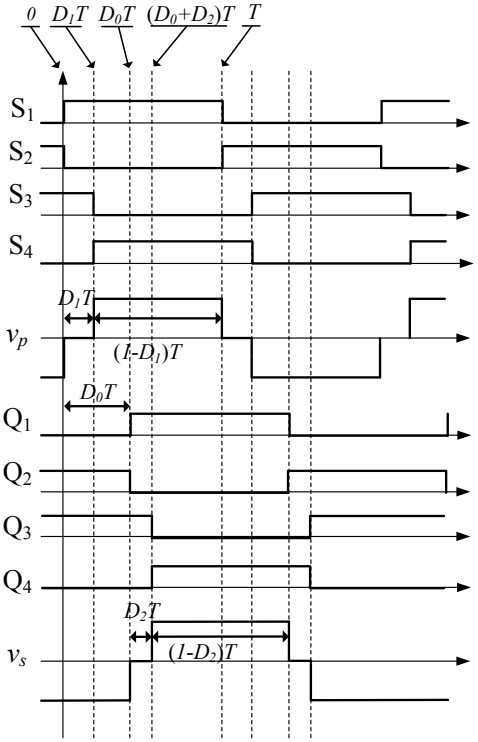

Fig.2 Typical waveform of PWM control

In fact, $v_p(t)$ is a three-level square wave, but it can be formed by adding two two-level square waves. We define the two-level square waves $S(t)$, and $S(t\text{-}DT)$ as shown in Fig. 3.

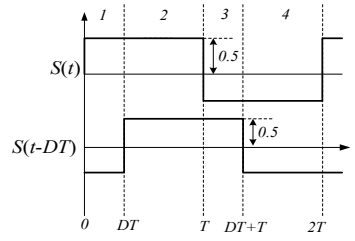

Fig. 3. Waveform of $S(t)$ and $S(t\text{-}DT)$

Then $v_p(t)$ can be represented by $v_p(t) = V_1\times[S(t)+ S(t\text{-}D_1T)]$, where V_1 is the peak value of $v_p(t)$, and is constant. Similarly, for the secondary side H bridge, the voltage $v_s(t)$ can also be represented as $nv_s(t) = V_2\times[S(t\text{-}D_0T)+ S(t\text{-}D_0T\text{-}D_2T)]$. For simplicity, V_2 is the peak value of $n\times v_s(t)$, wherein n is the turn ratio of the high frequency transformer. We denote $S(t)$, $S(t\text{-}D_1T)$, $S(t\text{-}D_0T)$ and $S(t\text{-}D_0T\text{-}D_2T)$ as $S_1(t)$, $S_2(t)$, $S_3(t)$ and $S_4(t)$ respectively. The equivalent circuits of DAB-IBDC are illustrated in Fig. 4.

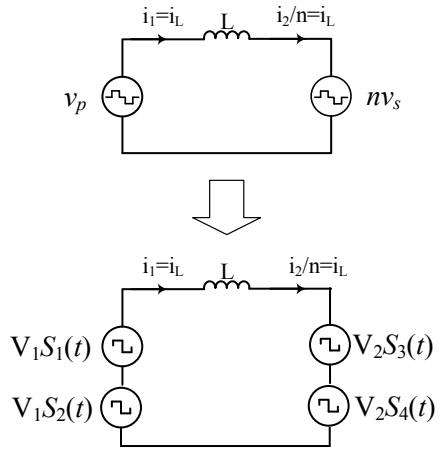

Fig. 4 Equivalent circuit of DAB-IBDC

There is only one state variable for the equivalent circuit of DAB-IBDC as in Fig.4. And the state equation can be obtained as

$$L\frac{di_L}{dt} = (v_p - nv_s) = [V_1(S_1(t)+S_2(t)) - V_2(S_3(t)+S_4(t))] \quad (1)$$

Solution of (1) is

$$i_L(t) = \frac{1}{L}\int [V_1(S_1(t)+S_2(t)) - V_2(S_3(t)+S_4(t))]dt \quad (2)$$

Because of the linearity of integration, we can split the integration in (2) into four similar parts, and every part is the integration of a square wave with different time delay. As we known, at steady state, the DC component of the inductor current is zero, so the integration of a two level square wave is a symmetrical bipolar triangle wave which is given in Fig.5. $Tr(t)$ is defined as the integration of $S(t)$.

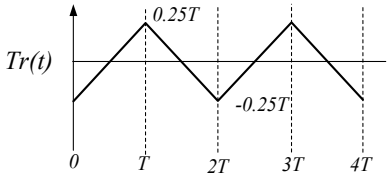

Fig.5 Waveform of $Tr(t)$

According to the property of integration

$$f(t) = \int g(t)dt \Rightarrow f(t-\mathrm{DT}) = \int g(t-\mathrm{DT})dt \quad (3)$$

The inductor current can be represented as

$$i_L(t) = \frac{1}{L}[V_1(Tr(t)+Tr(t-\mathrm{D_1T})) - V_2(Tr(t-\mathrm{D_0T})+Tr(t-(D_0+\mathrm{D_2})\mathrm{T}))] \quad (4)$$

It can be found that the inductor current is a summation of several triangle waves.

B. Analysis of Power Flow and Inductor Current

At steady state, $v_p(t)$, $v_s(t)$ and $i_L(t)$ have the property as

$$f(t) = -f(t+\mathrm{T}) \text{ and } f(t) = f(t+2\mathrm{T}) \tag{5}$$

where, $f(t)$ can be $v_p(t)$, $v_s(t)$ and $i_L(t)$. And we assume that all devices are ideal, losses are not considered, so the efficiency of the converter is 100%. By using (5), the average power which is transferred from primary side to the secondary side is

$$P = \frac{1}{T}\int_0^T [v_p(t)\,\mathrm{i}_L(t)dt = \frac{1}{T}\int_0^T [nv_s(t)\,\mathrm{i}_L(t)dt \tag{6}$$

Combining (4) and (6), the power flow P yields

$$\begin{aligned} P = {} & \frac{V_1^2}{\mathrm{T}L}\underbrace{\int_{D_1T}^{T}[Tr(t)+Tr(t-\mathrm{D}_1\mathrm{T})]dt}_{PA} \\ & -\frac{V_1V_2}{\mathrm{T}L}\underbrace{\int_{D_1T}^{T}[Tr(t-\mathrm{D}_0\mathrm{T})+Tr(t-(D_0+\mathrm{D}_2)\mathrm{T})]dt}_{PB} \end{aligned} \tag{7}$$

For the *PA* term of (7), upon collecting terms, one obtains

$$PA = [\frac{1}{4}(\mathrm{D}_1 - D_1^2) + \frac{1}{4}(D_1^2 - \mathrm{D}_1)]\mathrm{T}^2 = 0 \tag{8}$$

The *PA* term is zero for arbitrary D_0, D_1 and D_2. In fact, each term of *PA* describes the circulating power in the primary side H bridge, hence this power cannot be transferred to the secondary side. However, that circulating power may increase the losses of DAB-IBDC. And for the *PB* term,

$$PB = \underbrace{\int_{D_1T}^{T} Tr(\mathrm{t}-\mathrm{D}_0\mathrm{T})dt}_{PB1} + \underbrace{\int_{D_1T}^{T} Tr(\mathrm{t}-(D_0+\mathrm{D}_2)\mathrm{T})dt}_{PB2} \tag{9}$$

Because $Tr(t)$ is a piecewise function, there are different conclusions for different modes. Considering the operating waveforms for the converter, the relation modes among D_0, $\mathrm{D}_1$and D_2 can be divided into six categories, as given in Fig. 6. The Mode 2 and Mode 3 are not considered in [8]. The operating waveforms of the voltage across the inductor and the current of the inductor for each mode are illustrated in Fig. 6.

The PB term can be divided into two parts: PB1 and PB2. For the Mode 1, the PB1 and PB2 term are

$$\begin{aligned} PB1 = {} & \int_{D_1T}^{D_0T}(-\frac{1}{2}(t-\mathrm{D}_0\mathrm{T})-\frac{1}{4}\mathrm{T})dt + \int_{D_0T}^{T}(\frac{1}{2}(t-\mathrm{D}_0\mathrm{T})-\frac{1}{4}\mathrm{T})dt \\ PB2 = {} & \int_{D_1T}^{(D_0+D_2)T}(-\frac{1}{2}(t-(D_0+D_2)\mathrm{T})-\frac{1}{4}\mathrm{T})dt \\ & + \int_{D_0T}^{T}(\frac{1}{2}(t-(D_0+D_2)\mathrm{T})-\frac{1}{4}\mathrm{T})dt \end{aligned} \tag{10}$$

By adding PB1 to PB2, the power flow of DAB-IBDC at Mode 1 can be calculated

$$\begin{aligned} P = {} & \frac{-V_1V_2}{TL}(P_{B1}+P_{B2}) \\ = {} & \frac{-V_1V_2T}{L}(-D_0+{D_0}^2+0.5D_1-D_0D_1+0.5D_1^2-0.5D_2+D_0D_2-0.5D_1D_2+0.5{D_2}^2) \end{aligned} \tag{11}$$

Without calculating every turning point of the current waveform, the accurate power flow can be calculated directly. When D_1 and D_2 are zero, P is as follows,

$$P = \frac{V_1V_2T}{L}(1-\mathrm{D}_0)\mathrm{D}_0 \tag{12}$$

This is the power flow of so-called SPS (Single Phase Shift) control method [3], [4].

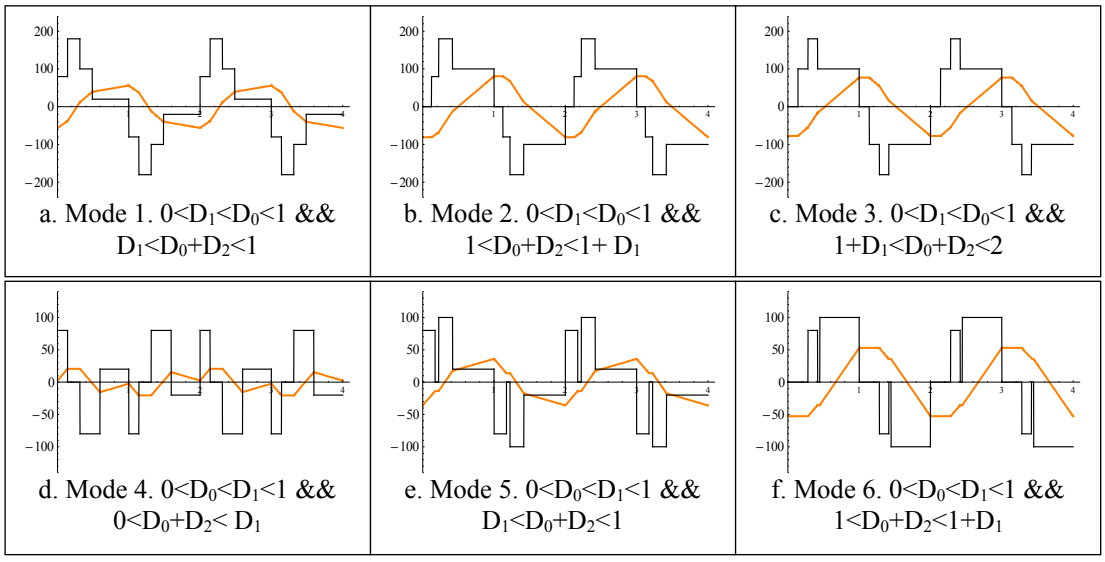

Fig. 6. Operating waveforms of voltage and current of the inductor for each mode

The RMS value of the inductor current can be calculated by similar method. At steady state, the inductor current satisfies the equations in (3) and (5), the RMS value is

$$I_{RMS}=\sqrt{\frac{1}{T}\int_0^T i(t)dt}= \sqrt{\frac{1}{TL^2}\int_0^T [\mathrm{V}_1(Tr(t)+Tr(t-\mathrm{D}_1\mathrm{T}))-\mathrm{V}_2(Tr(t-\mathrm{D}_0\mathrm{T})+Tr(t-(D_0+\mathrm{D}_2)\mathrm{T}))]^2 dt} \quad (13)$$

The integration in equation (13) is composed by two terms, the first is $\int Tr^2(t\text{-}x\mathrm{T})dt$, and the second is $\int Tr(t\text{-}yT)Tr(t\text{-}xT)dt$. Each term has uniform solution:

$$\begin{aligned}&\int_0^T Tr^2(t-xT)dt=\frac{0.0625}{3}T^3\\ &\int_0^T Tr(t-xT)Tr(t-yT)dt=\frac{0.25}{3}[0.25-1.5|\mathrm{x}-\mathrm{y}|^2+|\mathrm{x}-\mathrm{y}|^3]T^3\end{aligned} \quad (14)$$

By (14), the RMS value of inductor current can be written directly,

$$\begin{aligned}I_{RMS}^2=&\frac{T^2}{L^2}(\frac{0.125}{3}V_1^2+\frac{0.125}{3}V_2^2+\frac{0.5}{3}\left(0.25-1.5D_1^2+D_1^3\right)V_1^2\\ &-\frac{0.5}{3}\left(0.25-1.5D_0^2+D_0^3\right)V_1V_2+\frac{0.5}{3}\left(0.25-1.5D_2^2+D_2^3\right)V_2^2\\ &-\frac{0.5}{3}\left(0.25-1.5\left(D_0+D_2\right)^2+\left(D_0+D_2\right)^3\right)V_1V_2\\ &-\frac{0.5}{3}\left(0.25-1.5\left(D_0-D_1\right)^2+\left(D_0-D_1\right)^3\right)V_1V_2\\ &-\frac{0.5}{3}\left(0.25-1.5\left(D_0+D_2-D_1\right)^2+\left(D_0+D_2-D_1\right)^3\right)V_1V_2)\end{aligned} \quad (15)$$

For the traditional schemes used in [8], the RMS value of inductor current can be obtained by integrating the current waveforms piece by piece. Then the calculation is very complex. However, by the method proposed above, the details of inductor current waveform are not needed. RMS value of the inductor current is the combination of several similar terms, and these terms can be represented by the unified form. Hence the accurate conclusions can be computed without any other assumption.

By using the same manner, the conclusions of power flow and current for all the six modes are as below, shown in Table I.

TABLE I. THE POWER FLOW AND RSM VALUE OF INDUCTOR CURRENT FOR SIX MODES

Mode	Rang of D_0, D_1, D_2	
Mode 1	$0<D_1<D_0<1$ && $D_1<D_0+D_2<1$	$P=\frac{-V_1V_2T}{L}(-D_0+D_0^2+0.5D_1-D_0D_1+0.5D_1^2-0.5D_2+D_0D_2-0.5D_1D_2+0.5D_2^2)$ $I_{RMS}^2=\frac{T^2}{L^2}(\frac{0.125}{3}V_1^2+\frac{0.125}{3}V_2^2+\frac{0.5}{3}\left(0.25-1.5D_1^2+D_1^3\right)V_1^2-\frac{0.5}{3}\left(0.25-1.5D_0^2+D_0^3\right)V_1V_2$ $-\frac{0.5}{3}\left(0.25-1.5\left(D_0+D_2\right)^2+\left(D_0+D_2\right)^3\right)V_1V_2-\frac{0.5}{3}\left(0.25-1.5\left(D_0-D_1\right)^2+\left(D_0-D_1\right)^3\right)V_1V_2$ $-\frac{0.5}{3}\left(0.25-1.5\left(D_0+D_2-D_1\right)^2+\left(D_0+D_2-D_1\right)^3\right)V_1V_2+\frac{0.5}{3}\left(0.25-1.5D_2^2+D_2^3\right)V_2^2)$
Mode 2	$0<D_1<D_0<1$ && $1<D_0+D_2<1+D_1$	$P=-\frac{V_1V_2T}{L}(-0.5+0.5D_0^2+0.5D_1-D_0D_1+0.5D_1^2+0.5D_2-0.5D_1D_2)$ $I_{RMS}^2=\frac{T^2}{L^2}(\frac{0.125}{3}V_1^2+\frac{0.125}{3}V_2^2+\frac{0.5}{3}\left(0.25-1.5D_1^2+D_1^3\right)V_1^2-\frac{0.5}{3}\left(0.25-1.5D_0^2+D_0^3\right)V_1V_2-$ $\frac{0.5}{3}\left(0.25-1.5\left(2-D_0-D_2\right)^2+\left(2-D_0-D_2\right)^3\right)V_1V_2-\frac{0.5}{3}\left(0.25-1.5\left(D_0-D_1\right)^2+\left(D_0-D_1\right)^3\right)V_1V_2-$ $\frac{0.5}{3}\left(0.25-1.5\left(D_0+D_2-D_1\right)^2+\left(D_0+D_2-D_1\right)^3\right)V_1V_2+\frac{0.5}{3}\left(0.25-1.5D_2^2+D_2^3\right)V_2^2)$
Mode 3	$0<D_1<D_0<1$ && $1+D_1<D_0+D_2<2$	$P=\frac{V_1V_2T}{L}\left(-1+D_0-0.5D_1+1.5D_2-D_0D_2+0.5D_1D_2-0.5D_2^2\right)$ $I_{RMS}^2=\frac{T^2}{L^2}(\frac{0.125}{3}V_1^2+\frac{0.125}{3}V_2^2+\frac{0.5}{3}\left(0.25-1.5D_1^2+D_1^3\right)V_1^2-\frac{0.5}{3}\left(0.25-1.5D_0^2+D_0^3\right)V_1V_2-$ $\frac{0.5}{3}\left(0.25-1.5\left(2-D_0-D_2\right)^2+\left(2-D_0-D_2\right)^3\right)V_1V_2-\frac{0.5}{3}\left(0.25-1.5\left(D_0-D_1\right)^2+\left(D_0-D_1\right)^3\right)V_1V_2-$ $\frac{0.5}{3}\left(0.25-1.5\left(2-D_0-D_2+D_1\right)^2+\left(2-D_0-D_2+D_1\right)^3\right)V_1V_2+\frac{0.5}{3}\left(0.25-1.5D_2^2+D_2^3\right)V_2^2)$
Mode 4	$0<D_0<D_1<1$ && $0<D_0+D_2<D_1$	$P=\frac{V_1V_2T}{L}(-D_0+0.5D_1+D_0D_1-0.5D_1^2-0.5D_2+0.5D_1D_2)$

		$I_{RMS}^2=\frac{T^2}{L^2}(\frac{0.125}{3}V_1^2+\frac{0.125}{3}V_2^2+\frac{0.5}{3}\left(0.25-1.5D_1^2+D_1^3\right)V_1^2-\frac{0.5}{3}\left(0.25-1.5D_0^2+D_0^3\right)V_1V_2-$ $\frac{0.5}{3}\left(0.25-1.5\left(D_0+D_2\right)^2+\left(D_0+D_2\right)^3\right)V_1V_2-\frac{0.5}{3}\left(0.25-1.5\left(D_1-D_0\right)^2+\left(D_1-D_0\right)^3\right)V_1V_2-$ $\frac{0.5}{3}\left(0.25-1.5\left(D_1-D_0-D_2\right)^2+\left(D_1-D_0-D_2\right)^3\right)V_1V_2+\frac{0.5}{3}\left(0.25-1.5D_2^2+D_2^3\right)V_2^2)$
Mode 5	$0<D_0<D_1<1$ && $D_1<D_0+D_2<1$	$P=-\frac{V_1V_2T}{L}(-D_0+0.5D_0^2+0.5D_1-0.5D_2+D_0D_2-0.5D_1D_2+0.5D_2^2)$ $I_{RMS}^2=\frac{T^2}{L^2}(\frac{0.125}{3}V_1^2+\frac{0.125}{3}V_2^2+\frac{0.5}{3}\left(0.25-1.5D_1^2+D_1^3\right)V_1^2-\frac{0.5}{3}\left(0.25-1.5D_0^2+D_0^3\right)V_1V_2-$ $\frac{0.5}{3}\left(0.25-1.5\left(D_0+D_2\right)^2+\left(D_0+D_2\right)^3\right)V_1V_2-\frac{0.5}{3}\left(0.25-1.5\left(D_1-D_0\right)^2+\left(D_1-D_0\right)^3\right)V_1V_2-$ $\frac{0.5}{3}\left(0.25-1.5\left(D_0+D_2-D_1\right)^2+\left(D_0+D_2-D_1\right)^3\right)V_1V_2+\frac{0.5}{3}\left(0.25-1.5D_2^2+D_2^3\right)V_2^2)$
Mode 6	$0<D_0<D_1<1$ && $1<D_0+D_2<1+D_1$	$P=-\frac{V_1V_2T}{L}(-0.5+0.5D_1+0.5D_2-0.5D_1D_2)$ $I_{RMS}^2=\frac{T^2}{L^2}(\frac{0.125}{3}V_1^2+\frac{0.125}{3}V_2^2+\frac{0.5}{3}\left(0.25-1.5D_1^2+D_1^3\right)V_1^2-\frac{0.5}{3}\left(0.25-1.5D_0^2+D_0^3\right)V_1V_2-$ $\frac{0.5}{3}\left(0.25-1.5\left(2-D_0-D_2\right)^2+\left(2-D_0-D_2\right)^3\right)V_1V_2-\frac{0.5}{3}\left(0.25-1.5\left(D_1-D_0\right)^2+\left(D_1-D_0\right)^3\right)V_1V_2-$ $\frac{0.5}{3}\left(0.25-1.5\left(D_0+D_2-D_1\right)^2+\left(D_0+D_2-D_1\right)^3\right)V_1V_2+\frac{0.5}{3}\left(0.25-1.5D_2^2+D_2^3\right)V_2^2)$

III. Simulation and Experiment

In order to verify the above analysis, a simulating model was constructed in MATLAB R2014a. And a prototype of the DAB-IBDC was built in the laboratory. The parameters of prototype are shown in Table Ⅱ.

The comparison among the simulation results, experimental data and theoretic analysis is shown in Table Ⅲ. For resistive loads, the output power can be determined by the output voltage that is easier to be measured.

The corresponding experimental waveforms of inductor current and voltage for each mode are illustrated in Fig. 7.

TABLE II. Circuit Parameters of the Converter

Inductor *L*	**107.2μH**
Transformer Turn Raito *n*	**1:1**
DC Input Voltage	**80V**
Switching Frequency *f*	**20kHz**

TABLE III. Comparison of Theoretic Results, Simulation Results and Experimental Results

Mode	D_0	D_1	D_2	Load		Theory	Simulation	Experiment
Mode 1	0.3	0.2	0.4	20Ω	Voltage (V)	68.2	66.3	67
					Current RMS (A)	5.14	5.22	5.36
Mode 2	0.4	0.2	0.7	40Ω	Voltage (V)	70.9	69.7	69
					Current RMS (A)	6.17	6.35	6.76
Mode 3	0.4	0.1	0.75	40Ω	Voltage (V)	49.4	48.9	46
					Current RMS (A)	6.04	6.15	6.32
Mode 4	0.3	0.4	0.0	40Ω	Voltage (V)	43.0	43.4	43
					Current RMS (A)	1.76	1.78	1.68
Mode 5	0.2	0.3	0.4	40Ω	Voltage (V)	93.4	84.2	83
					Current RMS (A)	3.74	3.79	4.24
Mode 6	0.3	0.4	0.8	40Ω	Voltage (V)	43	42.9	45
					Current RMS (A)	4.43	4.35	4.43

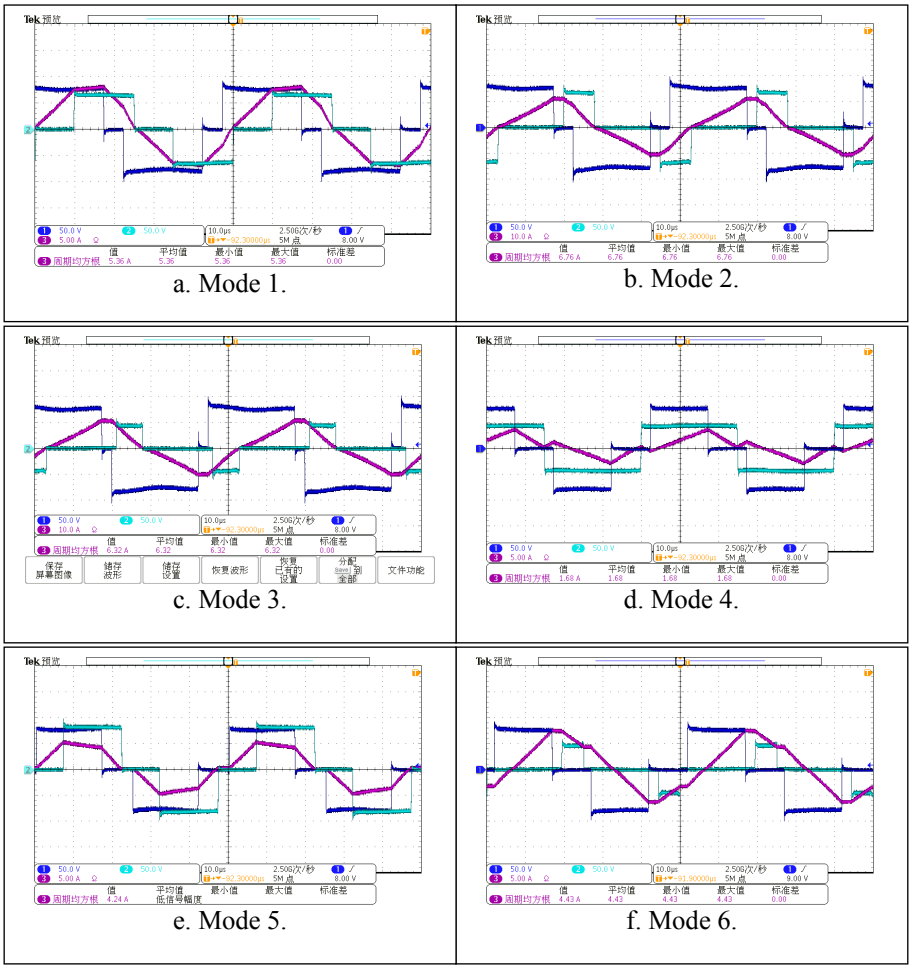

Fig. 7. Experimental waveforms of voltage and current of the inductor for each mode

According to the Table III, it can be seen that the theoretic results can accurately predict the power flow and the RMS value of the inductor current of DAB-IBDC.

IV. Conclusion

This paper presented detailed theoretic analysis of PWM control of DAB-IBDC. By taking apart the operating waveforms of primary side H bridge, and the secondary side H bridge into several uniform parts, it can be found that the current of inductor is a superposition of triangle waves. Due to the superposition principle of the circuits, by using simple waveforms to compose the complicated waveforms, the complexity of calculation of power flow and inductor current RMS value is reduced significantly. The theoretic results have good agreement to the simulation results and the experimental data.

References

[1] M. N. Kheraluwala, R. W. Gascoigne, D. M. Divan, and E. D. Baumann, "Performance characterization of a high-power dual active bridge DC-to-DC converter," *Ind. Appl. IEEE Trans. On*, vol. 28, no. 6, pp. 1294–1301, 1992.

[2] H. Akagi, T. Yamagishi, N. M. L. Tan, S. Kinouchi, Y. Miyazaki, and M. Koyama, "Power-Loss Breakdown of a 750-V 100-kW 20-kHz Bidirectional Isolated DC/DC Converter Using SiC-MOSFET/SBD Dual Modules," *IEEE Trans. Ind. Appl.*, vol. 51, no. 1, pp. 420–428, Jan. 2015.

[3] B. Zhao, Q. Song, W. Liu, and Y. Sun, "Overview of Dual-Active-Bridge Isolated Bidirectional DC-DC Converter for High-Frequency-Link Power-Conversion System," *IEEE Trans. Power Electron.*, vol. 29, no. 8, pp. 4091–4106, Aug. 2014.

[4] F. Krismer and J. W. Kolar, "Accurate Small-Signal Model for the Digital Control of an Automotive Bidirectional Dual Active Bridge," *IEEE Trans. Power Electron.*, vol. 24, no. 12, pp. 2756–2768, Dec. 2009.

[5] B. Zhao, Q. Song, W. Liu, and W. Sun, "Current-Stress-Optimized Switching Strategy of Isolated Bidirectional DC/DC Converter With Dual-Phase-Shift Control," *IEEE Trans. Ind. Electron.*, vol. 60, no. 10, pp. 4458–4467, Oct. 2013.

[6] W. Choi, K.-M. Rho, and B. H. Cho, "Fundamental Duty Modulation of Dual-Active-Bridge Converter for Wide Range Operation," *IEEE Trans. Power Electron.*, pp. 1–1, 2015.

[7] B. Zhao, Q. Song, W. Liu, G. Liu, and Y. Zhao, "Universal High-Frequency-Link Characterization and Practical Fundamental-Optimal Strategy for Dual-Active-Bridge DC-DC Converter Under PWM Plus Phase-Shift Control," *IEEE Trans. Power Electron.*, vol. 30, no. 12, pp. 6488–6494, Dec. 2015.

[8] A. K. Jain and R. Ayyanar, "Pwm control of dual active bridge: Comprehensive analysis and experimental verification," *IEEE Trans. Power Electron.*, vol. 26, no. 4, pp. 1215–1227, Apr. 2011.